# Clear-sky shortwave radiative closure for the Cabauw Baseline Surface Radiation Network site, Netherlands

Ping Wang,[1] Wouter H. Knap,[1] Peter Kuipers Munneke,[2] and Piet Stammes[1]

[1]   In this paper a clear-sky shortwave closure analysis is presented for the Baseline Surface Radiation Network (BSRN) site of Cabauw, Netherlands (51.97°N, 4.93°E). The analysis is based on an exceptional period of fine weather during the first half of May 2008, resulting in a selection of 72 comparisons, on 6 days, between BSRN measurements and Doubling Adding KNMI (DAK) model simulations of direct, diffuse, and global irradiances. The data span a wide range of aerosol properties, water vapor columns, and solar zenith angles. The model input consisted of operational Aerosol Robotic Network (AERONET) aerosol products and radiosonde data. The wavelength dependence of the aerosol optical thickness, single scattering albedo, and asymmetry parameter was taken into account. On the basis of these data, excellent closure was obtained: the mean differences between model and measurements are 2 W/m$^2$ (+0.2%) for the direct irradiance, 1 W/m$^2$ (+0.8%) for the diffuse irradiance, and 2 W/m$^2$ (+0.3%) for the global irradiance. The good results were obtained because of proper specification of the DAK model input and the high quality of the AERONET and BSRN measurements. The sensitivity of the achieved closure to uncertainties in the aerosol optical thickness, single scattering albedo, and asymmetry parameter was examined. Furthermore, several sensitivity experiments related to the wavelength dependence of the aerosol optical properties and the treatment of water vapor were performed. It appeared that a correct description of the wavelength dependence of the aerosol optical properties is important for achieving broadband closure. However, broadband closure can also be obtained by means of using spectrally averaged values of the single scattering albedo and the asymmetry parameter. Cancellation of errors in different parts of the solar spectrum also contributes to the achieved closure.

## 1.   Introduction

[2]   During the last two decades, several attempts have been made to achieve agreement between clear-sky shortwave broadband irradiance models and surface measurements of direct and diffuse irradiance [e.g., *Kato et al.*, 1997; *Halthore et al.*, 1997; *Halthore and Schwartz*, 2000; *Barnard and Powell*, 2002; *Henzing et al.*, 2004]. In general, models and measurements agreed well for the direct component but closing the gap for diffuse irradiances remained problematic. In the course of time, however, instrumental problems, related to pyranometer thermal offsets, were solved and model input improved in such a way that *Michalsky et al.* [2006] were able to present better results than previously achieved. The authors report biases between models and measurements of generally less than

1% for direct irradiances and less than 1.9% for diffuse irradiances. A recent study performed by *Nowak et al.* [2008], however, demonstrates that closure can still be a challenge; the authors find biases of −1.8% for direct irradiances and 5.2% for diffuse irradiances. In general, the number of studies reporting a satisfactory degree of closure for both direct and diffuse irradiances is still limited, which motivated us to perform the study presented here.

[3]   In this paper a clear-sky shortwave closure analysis is presented for the Baseline Surface Radiation Network (BSRN) site of Cabauw, Netherlands (51.97°N, 4.93°E). The analysis is based on an exceptional period of fine weather in the first half of May 2008 during the Intensive Measurement Period At the Cabauw Tower (IMPACT), an activity of the European Integrated project on Aerosol Cloud Climate and Air Quality Interactions (EUCAARI). Although IMPACT produced a wealth of data, it was decided to conduct the closure analysis using routine measurements only, provided by BSRN and the Aerosol Robotic Network (AERONET), completed with radiosonde observations. The rationale for this pragmatic approach is the possibility of applying the method presented here to

---

[1]Royal Netherlands Meteorological Institute, De Bilt, Netherlands.
[2]Institute for Marine and Atmospheric Research, Utrecht University, Utrecht, Netherlands.

other periods and (BSRN) sites, where routine measurements are readily available, without having to deal with the investments and restrictions of an intensive observation period.

[4] For the simulation of the BSRN radiation measurements the Doubling Adding KNMI (DAK) model was used [*De Haan et al.*, 1987; *Stammes et al.*, 1989; *Stammes*, 2001]. The DAK model, which includes multiple scattering and polarization, is based on the doubling-adding method which allows for an accurate treatment of scattering and absorption in a multilayer atmosphere. It is the first time that the doubling-adding method has been used for a closure study.

[5] The organization of this paper is as follows. First, the DAK radiative transfer model is described (section 2). In section 3 the input for the radiative transfer model and the BSRN radiation measurements are described. Section 4 describes the results in terms of comparisons between model calculations and measurements of irradiances. A discussion of the results on the basis of a sensitivity analysis is given in the same section. Conclusions are drawn in section 5.

## 2. Radiative Transfer Model

[6] In the DAK model the atmosphere is assumed to be composed of a stack of (different) plane-parallel layers, on top of a reflecting surface. Each layer is homogeneous. The atmospheric state (pressure, temperature, trace gas mixing ratio) and optical properties of particles (optical thickness, single scattering albedo, phase matrix) are defined for each layer individually. In the doubling-adding scheme, integrations of products of radiation field matrices, like reflection and transmission matrices, take place [*De Haan et al.*, 1987]. The azimuth dependence of the radiation field is treated as a Fourier expansion, so each Fourier term can be treated separately. Since in this paper irradiances are needed, only the zeroth-order Fourier term is calculated.

[7] The zenith angle integration is treated as a Gaussian integration. Using special matrix weights, the doubling-adding scheme can be reduced to repeated matrix multiplications only. The number of Gaussian division points determines the accuracy of doubling-adding. For the calculations presented in this paper, 12 Gaussian points were used to achieve an accuracy of $10^{-5}$.

[8] In its original line-by-line configuration, the DAK model has been widely used for satellite retrievals [*Knap et al.*, 2002, 2005; *Acarreta et al.*, 2004; *Veefkind et al.*, 2006; *Veihelmann et al.*, 2007; *Boersma et al.*, 2008; *Roebeling et al.*, 2008]. Recently, the model has been made suitable for broadband simulations by means of implementation of the correlated-k method for gaseous absorption [*Kuipers Munneke et al.*, 2008] using the approach described by *Kato et al.* [1999]. The latter authors subdivided the solar spectrum into 32 wavelength bands, between 240 and 4600 nm, which closely follow the absorption bands of $H_2O$, $CO_2$, $O_2$ and $O_3$. For the calculations presented here, the solar spectrum has been taken from *Gueymard* [2004], which adds up to a total solar irradiance of 1366 W/m$^2$.

[9] Different options for the wavelength dependence of aerosol properties in the DAK model have been implemented by *Wang et al.* [2009]. In the model it is possible to

use Henyey-Greenstein phase functions or Mie phase functions (or phase functions derived from ray-tracing techniques) to describe single scattering. The most practical option consists of using Henyey-Greenstein phase functions and the specification of the aerosol optical depth, the single scattering albedo and the asymmetry parameter at each wavelength. If Mie phase functions are used, the expansion coefficients of the phase matrix can be given at each wavelength and the optical thickness is scaled to a reference wavelength by means of the spectral extinction coefficients. For the simulations presented in this paper, however, Henyey-Greenstein phase functions were used.

[10] For evaluation purposes, the broadband version of DAK has been compared with SMARTS (Simple Model of the Atmospheric Radiative Transfer of Sunshine) [*Gueymard*, 2001] for cloudless model atmospheres [*Wang et al.*, 2009]. SMARTS performed well in the *Michalsky et al.* [2006] comparisons. For a pure Rayleigh atmosphere the differences between DAK and SMARTS for direct and diffuse irradiances are within 5 W/m$^2$. For atmospheres containing LOWTRAN aerosols the differences are within 10 W/m$^2$. *Wang et al.* [2009] attribute the differences to the fact that the settings of aerosol optical properties in SMARTS and DAK are not identical. The aerosol optical properties in SMARTS are based on fitting tabulated data, whereas DAK uses original tables. This also implies that the model specification of aerosol properties is crucial; a small difference in spectral aerosol properties may lead to large differences in simulated irradiances.

## 3. Model Input, Radiation Measurements, and Selection of Data

### 3.1. Model Input

[11] The key quantities needed to run the DAK model in clear-sky mode are the aerosol optical properties and their wavelength dependence, water vapor and ozone columns, and the surface albedo. These will be described in turn.

[12] The aerosol optical depth (AOD) and Ångström coefficients were taken from the AERONET Level 1.5 data for Cabauw [*Dubovik et al.*, 2000]. The single scattering albedo ($\omega_0$) and the asymmetry parameter (g) were taken from the AERONET inversion data. The AERONET Level 1.5 data are available about every 15 min. The single scattering albedo and the asymmetry parameter are retrieved about 10 times per day, but not between 10 and 13 UT. Therefore, linear interpolation techniques were used to obtain $\omega_0$ and g at selected AOD measurement times.

[13] In order to run DAK for the 32 wavelength intervals, the AOD, $\omega_0$, and g, were specified as a function of wavelength according to the interpolations and extrapolations shown in Figure 1. For Cabauw, AERONET gives these quantities for 440, 675, 870, and 1020 nm. For wavelengths between 440 and 1020 nm, the AOD was interpolated using the standard Ångström relation (AOD $\sim \lambda^{-\alpha}$, where $\lambda$ is the wavelength and $\alpha$ the Ångström coefficient) fitted to the four wavelengths. For wavelengths shorter than 440 nm and longer than 1020 nm, the 440–675 nm and 675–870 nm Ångström coefficients (provided by AERONET), respectively, were used to extrapolate the AOD. Between 440 and 1020 nm, $\omega_0$ and g were linearly interpolated. Outside the AERONET wavelength range, $\omega_0$
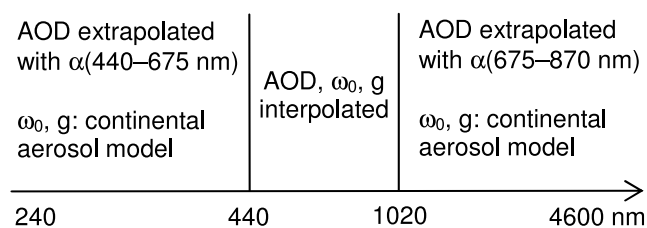
**Figure 1.** Spectral interpolation and extrapolation procedures for the aerosol optical depth (AOD), single scattering albedo ($\omega_0$), and asymmetry parameter (g). The Ångström coefficient is denoted by $\alpha$.

and g were taken from a wavelength-dependent continental aerosol model [*Deepak and Gerber*, 1983] and interpolated to the DAK wavelength grid. The continental model was taken because trajectory analyses showed predominant continental origin of air masses during the observation period. In the model atmospheres, all aerosol was put in the lowest layer, between 0 and 1 km, and it was assumed that the aerosol was well mixed.

[14] During the IMPACT intensive observation period radiosondes were launched at 0500, 1000 and 1600 UTC, giving vertical profiles of temperature, pressure, and relative humidity up to an altitude of about 12 km. Above this altitude the atmospheric profile was filled up with the midlatitude summer atmospheric profile given by *Anderson et al.* [1986]. For the DAK simulations at times between the radiosonde launches, profiles of the closest launch were used. The profiles of relative humidity were regridded to the DAK layer profile (32 layers, 1 km per layer up to a height of 25 km) and, more importantly, they were all scaled to equal the AERONET water vapor columns. So, every DAK simulation presented in the next section was made with the AERONET water vapor column as input.

[15] Total ozone columns were provided by the Ozone Monitoring Instrument (OMI, NASA Aura mission) via the Tropospheric Emission Monitoring Internet Service (TEMIS; http://www.temis.nl). One ozone column value per day was used. Since the Cabauw area is dominated by grass land, the surface albedo used in DAK has been derived from a typical grass curve [*Bowker et al.*, 1985]. The dependence of the surface albedo on the solar zenith angle was not taken into account (see also section 4.3).

### 3.2. Radiation Measurements and Selection of Data

[16] Cabauw has been part of the BSRN network since 2006. This means that the radiation measurements used for the closure study presented here were made according to the highest available standards [*Ohmura et al.*, 1998; *McArthur*, 2004]. The estimated uncertainties in the direct, diffuse, and global irradiance, as achieved by BSRN in 1995, are 2 W/m$^2$, 5 W/m$^2$, and 5 W/m$^2$, respectively. These values represent calibration uncertainties, which means that operational uncertainties, referring to field conditions, are generally larger. *Shi and Long* [2002] estimated the operational uncertainties for BSRN-type measurements to be typically $14 \pm 6$ W/m$^2$ for the direct irradiance and $9 \pm 3$ W/m$^2$ for the diffuse irradiance. For the ARM facility, *Stoffel* [2005] give the following estimates of 2-sigma uncertainties for the direct, diffuse, and global irradiance: 3% or 4 W/m$^2$

(whichever is larger), 6% or 20 W/m$^2$, and 6% or 10 W/m$^2$, respectively. Although these uncertainties are most probably instrument and site specific, they give reasonable estimates of what one might expect in the field.

[17] The direct and diffuse irradiance measurements in Cabauw were obtained with a Kipp & Zonen CH1 pyrheliometer and CM22 pyranometer, respectively. The CH1 was calibrated on site using the HF27159 absolute cavity radiometer which participated in the 10th International Pyrheliometer Comparison (IPC-X) [*Finsterle*, 2006]. The CM22 was shaded, ventilated, and slightly heated and its calibration is traceable to the World Radiometric Reference. No offset corrections were applied to diffuse irradiances. The direct irradiance was measured normal to the solar beam and the global irradiance ($E_{glo}$) was calculated from measurements of the direct and diffuse irradiance ($E_{dir}$ and $E_{dif}$, respectively) by means of: $E_{glo} = \mu_0 E_{dir} + E_{dif}$, where $\mu_0$ is the cosine of the solar zenith angle.

[18] In total 6 cloudless days (5 and 7–11 May 2008) were selected by means of situ observations by the human eye, images of a total sky imager, and backscatter measurements made by a Raman lidar operated by the National Institute for Public Health and the Environment (RIVM; see K. M. Wilson et al., CAELI—A multi-wavelength Raman lidar for the diurnal observation of clouds, aerosol and water vapour profiles and boundary layer structures, paper presented at the 24th International Laser Radar Conference, International Radiation Commission, Boulder, Colorado, 2008). Since only a limited number of AERONET inversions is available per day, and to reduce the computational time needed for the DAK simulations, only calculations for selected times were made. Generally, we have about 12 cases per day, adding up to a total of 72 cases during the 6 cloudless days. Each case consists of 1-min average BSRN irradiances [*Knap*, 2008]. The selected cases are evenly distributed over the days and follow significant changes in water vapor column and AOD.

[19] Figure 2 shows the daily variations of direct, diffuse, and global radiation, aerosol optical depth and water vapor column. Figure 3 shows the single scattering albedo, asymmetry parameter, aerosol optical depth, and water vapor column for the selection of 72 cases. For the selected cases, the variations are considerable; the AOD at 555 nm varies between 0.08 and 0.27 and the water vapor column varies between 0.65 and 1.72 cm. The same statement applies to the single scattering albedo and asymmetry parameter: $\omega_0$ ranges between 0.85 and 0.99 and g ranges between 0.61 and 0.71. The AERONET inversion data were not available between 1000 and 1300 UTC, so the single scattering albedo and asymmetry parameters had to be interpolated between these times. This may have caused some degree of error for cases where the variation in the quantities was large. Most probably, the single scattering albedo for cases 28 and 29 (values close to 0.99) is too high.

[20] For the 72 cases, the ozone column (not shown) varied between 320 and 360 Dobson units. The ranges of the three components of irradiance are 391–907 W/m$^2$ (direct), 55–147 W/m$^2$ (diffuse), and 150–858 W/m$^2$ (global). The corresponding mean values are 751 W/m$^2$, 106 W/m$^2$, and
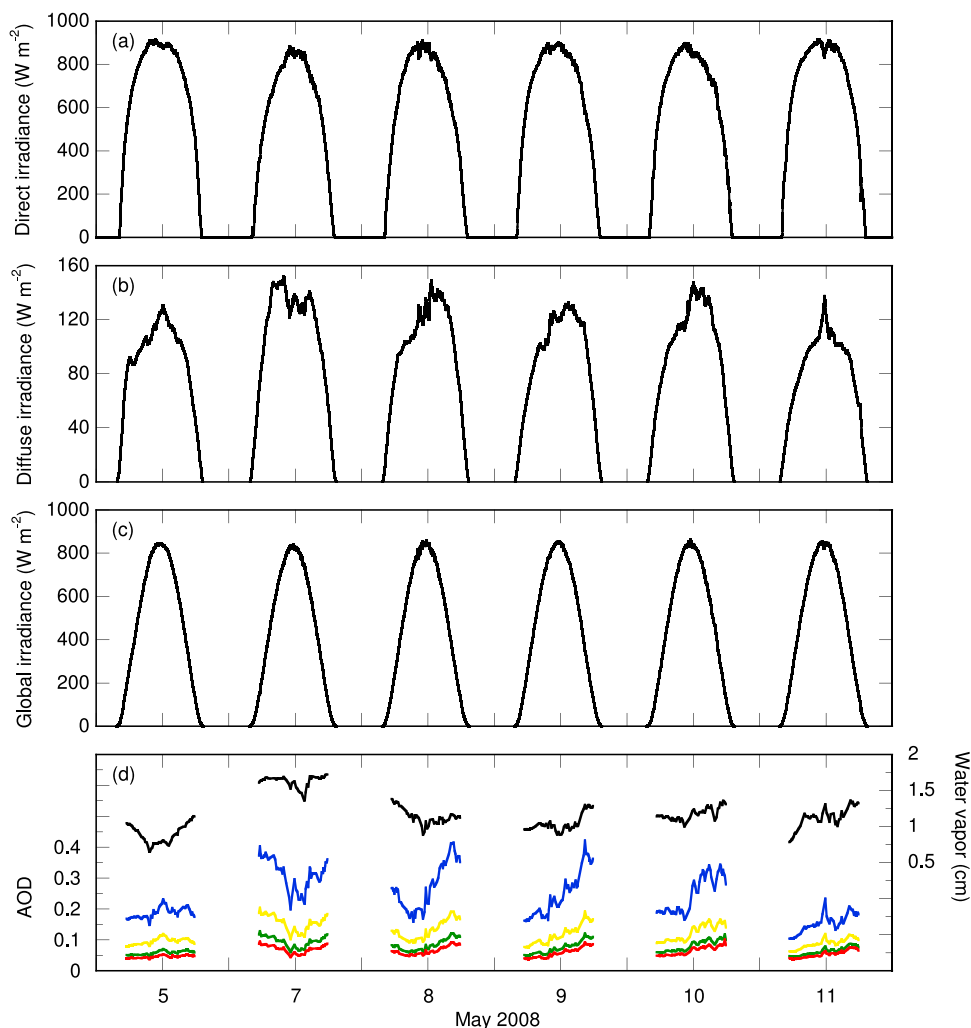
**Figure 2.** Daily variations in (a) direct irradiance, (b) diffuse irradiance, (c) global irradiance, and (d) AERONET water vapor column and aerosol optical depth (AOD) for 5 and 7−11 May 2008. The water vapor column is indicated by the black curve. The AOD is given for four AERONET wavelengths: 440 nm (blue), 675 nm (yellow), 870 nm (green), and 1020 nm (red). The 72 selected cases used for the closure study follow significant changes in water vapor column and AOD.

580 W/m$^2$, respectively. The solar zenith angle ranged between 42° and 76°.

## 4. Results

### 4.1. Comparison Between Simulations and Measurements

[21] The left panels of Figures 4a−4c show scatterplots of all DAK simulations versus BSRN measurements of the direct, diffuse, and global irradiance. The scatterplots, with the one-to-one lines indicated, show that there are excellent correlations for the three components of radiation. The differences between simulations and measurements are also shown in the right panels of Figures 4a−4c. The absolute range in the model−measurement difference is between −5 W/m$^2$ and +11 W/m$^2$ for the direct irradiance, between −4 and +9 W/m$^2$ for the diffuse irradiance, and between −3 and +11 W/m$^2$ for the global irradiance. In percent differences, these ranges are: −1.4% to +1.6%, −3.9% to +8.5%, and −1.4% to +2.7%, respectively. The mean differences

are 2 W/m$^2$ (+0.2%) for the direct irradiance, 1 W/m$^2$ (+0.8%) for the diffuse irradiance, and 2 W/m$^2$ (+0.3%) for the global irradiance. The sample standard deviations are small: 3 W/m$^2$, 2 W/m$^2$, and 3 W/m$^2$, respectively.

[22] By considering the operational measurement uncertainties (see section 3.2), the DAK simulations fall well within the uncertainty ranges of the BSRN measurements. Even if only calibration uncertainties are considered, there is, on average, near-perfect agreement between the simulations and measurements. Moreover, if one takes into account that the simulations also carry a certain degree of uncertainty (owing to uncertainties in aerosol optical properties, water vapor column, surface albedo, etc.), the general conclusion is that excellent closure was obtained between model and measurements of shortwave broadband irradiances. The results presented here are comparable to, or slightly better than, the results obtained by *Michalsky et al.* [2006] for the southern Great Plains site in Oklahoma, USA, during the 2003 aerosol intensive observation period. We believe that our good results were obtained because of
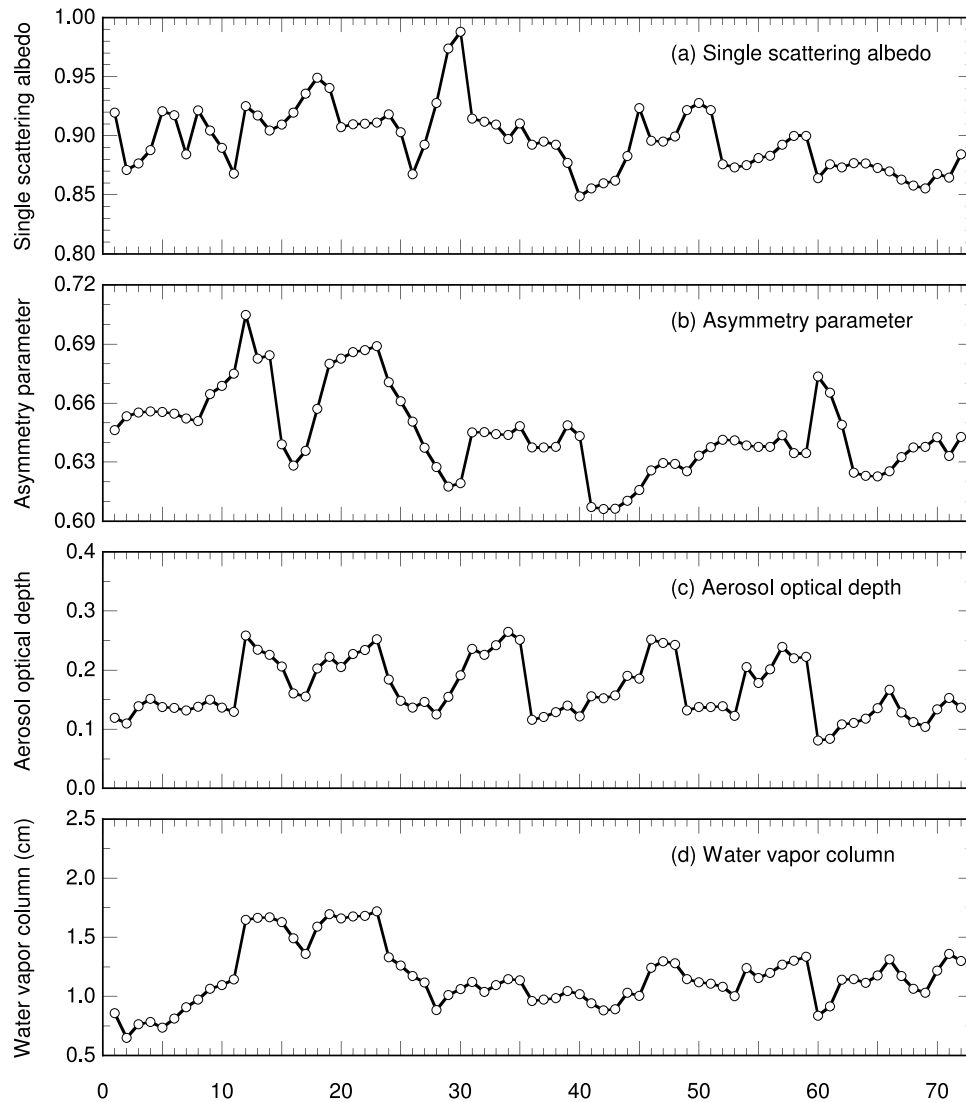
**Figure 3.** (a) Single scattering albedo, (b) asymmetry parameter, (c) aerosol optical depth (all at 555 nm), and (d) water vapor column for the 72 cases.

proper specification of the DAK model input and the high quality of the AERONET and BSRN measurements.

[23] In order to investigate the robustness of the closure presented here, several sensitivity experiments were performed. The first set of experiments consists of the sensitivity of the difference between simulations and measurements to uncertainties in aerosol optical depth, single scattering albedo, and asymmetry parameter. The second set of experiments takes a closer look at the assumptions made related to the spectral behavior of the aerosol optical properties and to the water vapor column. The two sets of experiments are described in the following two sections.

## 4.2. Sensitivity to Uncertainties in Aerosol Optical Properties

[24] For a representative subset of the 72 cases (case numbers 11−22 on 7 May 2008), wavelength-independent offsets of ±0.02, ±0.1, ±0.1 were applied to AOD, $\omega_0$, and g, respectively. Figures 5a−5d show the effects of these offsets

on the differences between simulations and measurements of the direct and diffuse irradiance. The effect of AOD ± 0.02 has a considerable negative effect on the achieved closure (Figures 5a and 5b): the increase and decrease in AOD gives mean differences for the direct irradiance of −25 W/m² and +28 W/m², respectively. For the diffuse irradiance the mean differences are +8 W/m² (for AOD + 0.02) and −9 W/m² (for AOD − 0.02). A measurement uncertainty in the AOD of 0.02 can be considered as a worst case limit; more likely the uncertainty is around 0.01 or less [*Nyeki et al.*, 2009]. Since the effect of a small AOD offset on the irradiance is more or less linear, the effect of AOD ± 0.01 is about half of the values mentioned before. The effect on the achieved closure is still negative for AOD ± 0.01.

[25] Changes in the single scattering albedo and asymmetry parameter only affect the diffuse irradiance (Figures 5c and 5d). The effects of $\omega_0$ ± 0.1 and g ± 0.1 on the achieved closure are also unfavorable and increase the mean differences between simulations and measurements to +12 and −13 W/m² ($\omega_0$ ± 0.1) and +5 and
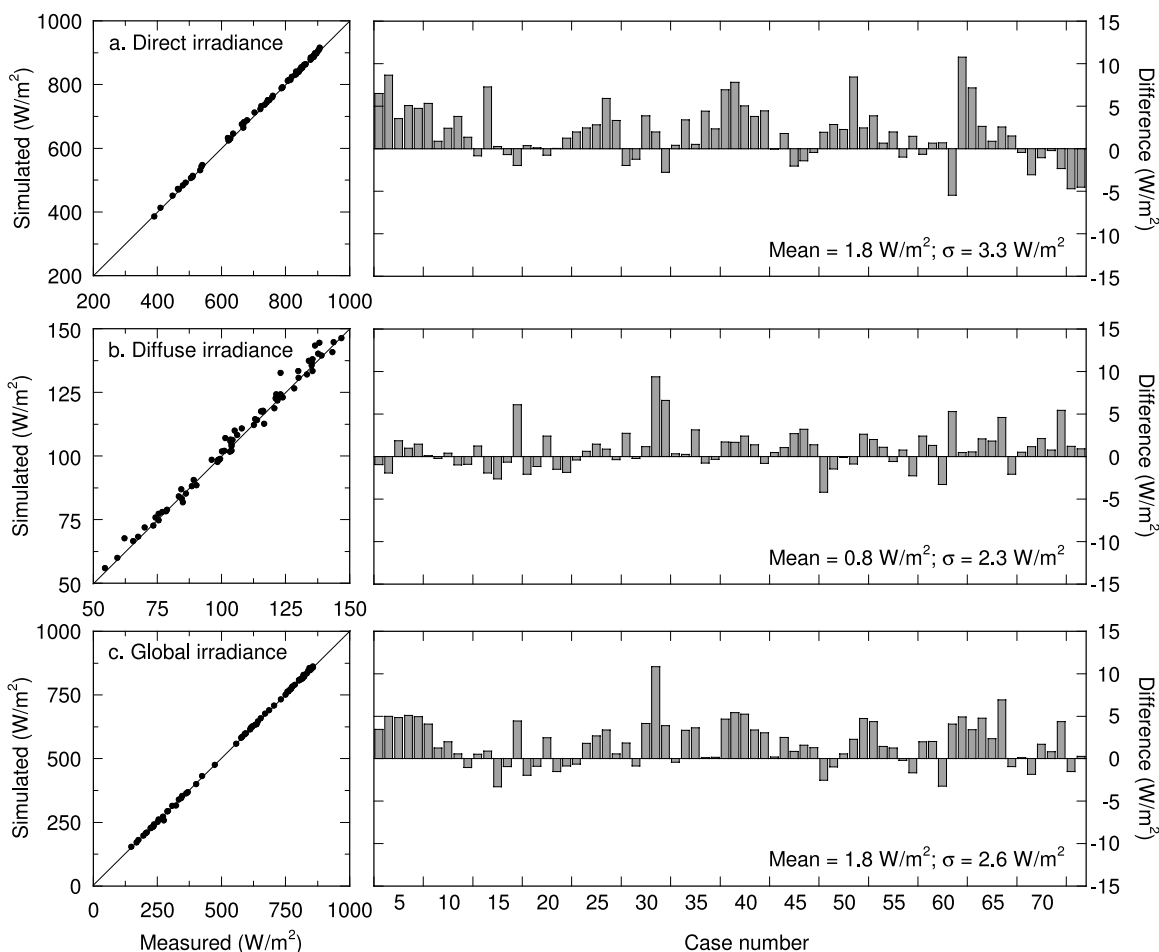
**Figure 4.** (a) Scatterplot of DAK simulations versus BSRN measurements of direct irradiance for 72 cases (left panel) and differences between DAK simulations and BSRN measurements of direct irradiance (right panel). (b) The same as in Figure 4a but for diffuse irradiance. (c) The same as in Figure 4a but for global irradiance.

−5 W/m$^2$ (g ± 0.1). If the single scattering albedo increases, the aerosols absorb less radiation so that more radiation is scattered, which increases the diffuse irradiances. If the asymmetry parameter increases, more radiation is scattered in the forward direction, so that more diffuse radiation reaches the surface. Similar reasoning can be given to explain the decreases in the diffuse radiation shown in Figures 5c and 5d.

### 4.3. Experiments on Aerosol Spectral Behavior and Water Vapor Column

[26] In order to investigate the assumptions described in section 3.1, four sensitivity experiments were performed. The experiments comprise: (1) changing the AOD by means of using a single Ångström coefficient (derived from the four AERONET wavelengths) instead of three coefficients, (2) using the AERONET four-wavelength average $\omega_0$ for all 32 wavelength bands, (3) similar as experiment 2 but for g, and (4) using only radiosonde water vapor columns. Experiments 2 and 3 imply wavelength independence of $\omega_0$ and g, and the exclusion of using the continental aerosol model. Experiment 4 is based on the use of only three water vapor columns per day (derived from the closest radiosonde

profile) instead of using the more frequently available AERONET columns.

[27] The results of the experiments are listed in Table 1. The first three experiments only slightly changed the differences between simulations and measurements. With respect to experiment 1, it appeared that the Ångström coefficients derived from the 440–675 nm and 675–870 nm pairs are different from the four-wavelength Ångström coefficient. It was also found that the AODs slightly deviate from the ideal Ångström relation. The experiment, however, learned that using a single four-wavelength Ångström coefficient does not significantly change the results, which suggests the presence of some spectral compensation effect. If the AOD measurements are accurate, the interpolation of the AOD based on a single Ångström coefficient is adequate and may even reduce errors because four wavelengths are used. The use of different Ångström coefficients is more accurate in cases where the Ångström relation is not exactly (or not at all) satisfied.

[28] Experiments 2 and 3 slightly improve the closure for the diffuse (and global) irradiance. The standard deviations, however, are slightly larger as compared to the reference case. This also suggests cancellation of errors for different
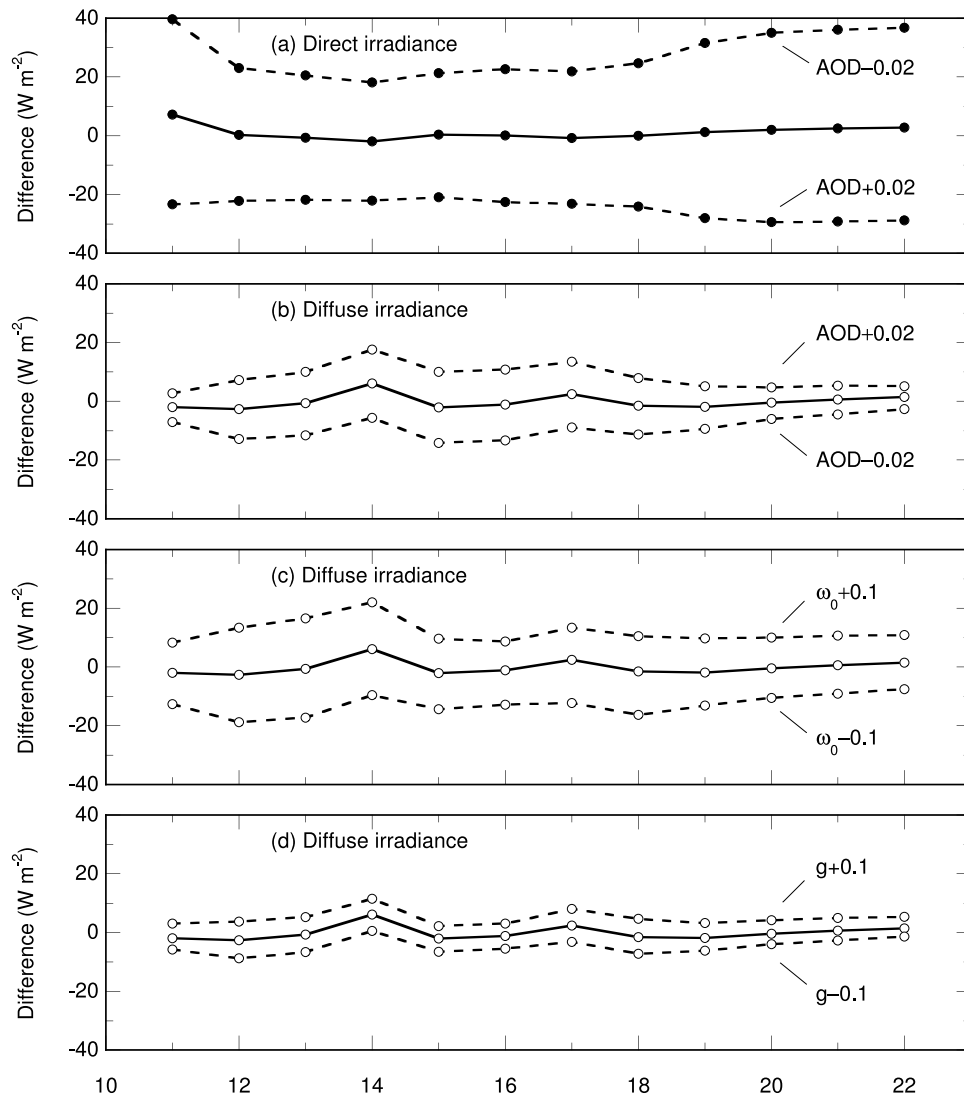
**Figure 5.** Differences between DAK simulations and BSRN measurements for the reference case (solid lines) and for changes (dashed lines) in aerosol optical depth (AOD), single scattering albedo ($\omega_0$), and asymmetry parameter (g). (a) AOD $\pm$ 0.02 (direct irradiance), (b) AOD $\pm$ 0.02 (diffuse irradiance), (c) $\omega_0$ $\pm$ 0.1 (diffuse irradiance), and (d) g $\pm$ 0.1 (diffuse irradiance).

parts of the irradiance spectrum. According to Mie theory, the single scattering albedo and the asymmetry parameter are determined by the size distribution of the aerosols, the complex refractive index and the ratio of wavelength and aerosol size. Therefore, theoretically, the single scattering albedo and the asymmetry parameter should depend on the wavelength. If $\omega_0$ or g are set to wavelength-independent values, it is likely that overestimation of the diffuse irradi-

ance (caused by overestimation of $\omega_0$ or g) at certain wavelengths is compensated by underestimation of the diffuse irradiance (caused by underestimation of $\omega_0$ or g) at other wavelengths. The cancellation of errors related to experiments 2 and 3 is demonstrated in Figure 6. The figure clearly shows cancellation of errors between visible and near-infrared wavelengths.

**Table 1.** Mean Differences Between DAK Simulations and BSRN Measurements of the Direct, Diffuse, and Global Irradiance for the Reference Case and four Different Sensitivity Experiments[a]

| | Direct ($\sigma$) | Diffuse ($\sigma$) | Global ($\sigma$) |
|---|---|---|---|
| Reference | +1.8 (3.3) | +0.8 (2.3) | +1.8 (2.6) |
| Experiment 1: one Ångström coefficient | +1.1 (3.2) | +1.1 (2.3) | +1.6 (2.6) |
| Experiment 2: average single scattering albedo | +1.8 (3.3) | +0.5 (3.0) | +1.5 (3.3) |
| Experiment 3: average asymmetry parameter | +1.8 (3.3) | −0.2 (2.4) | +0.8 (2.8) |
| Experiment 4: only radiosonde water vapor | −1.5 (5.8) | +0.7 (2.3) | −0.6 (4.0) |

[a] See section 4.2. The sample standard deviations are indicated by $\sigma$. All values are in W/m$^2$.
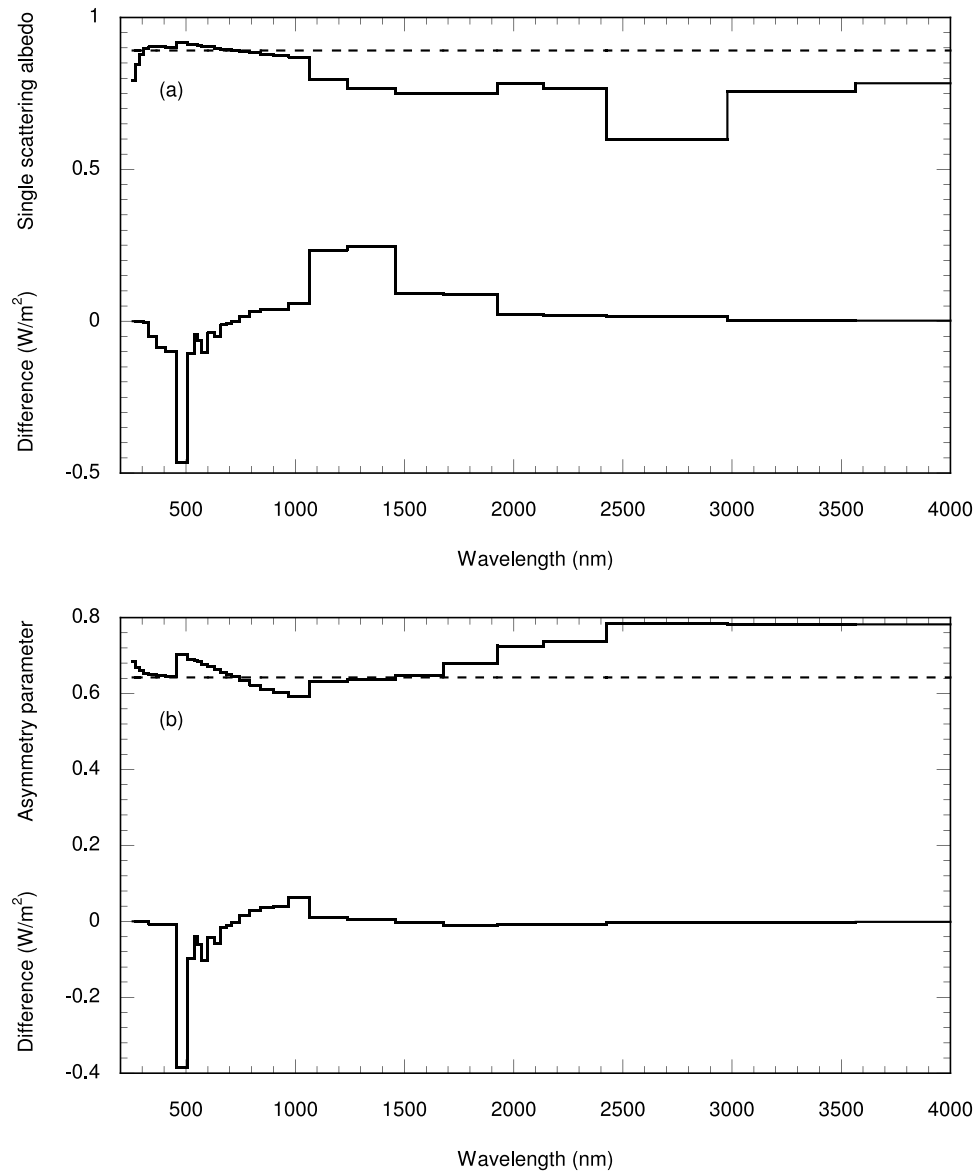
**Figure 6.** Effect of using wavelength-independent aerosol optical properties on simulations of diffuse irradiance: (a) experiment with average single scattering albedo (see experiment 2 in Table 1) and (b) experiment with average asymmetry parameter (see experiment 3 in Table 1). The two upper curves in Figures 6a and 6b represent the wavelength-dependent single scattering albedo and asymmetry parameter (solid lines) and the wavelength-average single scattering albedo and asymmetry parameter (dashed lines). The lower curves represent the difference in spectral diffuse irradiance between simulations with wavelength-average $\omega_0$ or g and simulations with wavelength-dependent $\omega_0$ or g.

[29] The wavelength dependence of $\omega_0$ and g should also be considered in view of the distribution of solar energy over the solar spectrum. The solar energy in the intervals 240–440 nm, 440–1020 nm and 1020–4600 nm is about 14.8%, 57.8% and 27.4%, respectively, of the solar energy between 240 and 4600 nm. At wavelengths where $\omega_0$ and g deviate most from the average, there is not much solar energy, and the contribution to the broadband irradiances is not significant. In this respect it is worth mentioning that using the continental aerosol model (or any other reasonable aerosol model) outside the AERONET wavelength range (see section 3.1) has little effect on the achieved closure because the AERONET values of $\omega_0$ and g are situated in those parts of the spectrum where most of the solar energy is present. In general, one can state that spectral cancellation of errors may hide some problems related to aerosol properties (but also gas absorptions) as treated in a radiative transfer model. To further consider the issue of the spectral cancellation of errors, spectral irradiance measurements are highly desirable, as was also pointed out by *Michalsky et al.* [2006].

[30] The only serious effect of the experiments presented in this subsection is obtained by not using the AERONET water vapor columns; experiment 4 shows that for the direct irradiance the difference changes sign and the standard deviation roughly doubles. Since water vapor primarily

absorbs in the near-infrared, where the diffuse irradiance is small, the effect of changing water vapor on the simulated diffuse irradiance is negligible. Besides, there appears to be no cancellation effect related to the influence of water vapor on the diffuse irradiance. The increase in the standard deviation for the direct irradiance is due to the fact that water vapor is highly variable throughout the day, which implies that it is better to use the more frequently available AERONET columns instead of only using the three values derived from the radiosonde profiles.

[31] Numerous other experiments can be performed to study the sensitivity of simulated irradiances, but the most important were described above. Changing the boundary layer height has negligible effect on the simulations and uncertainty in the surface albedo has an effect of less than 2 W/m$^2$ on the diffuse irradiance. *Henzing et al.* [2004] found an effect of ±2 W/m$^2$ on the diffuse (and global) irradiance if the (broadband) surface albedo is changed by ±0.03. Since the surface albedo generally shows a distinct increase with increasing solar zenith angle, it can be expected that the difference between simulated and measured diffuse (and global) irradiances correlates with the solar zenith angle. Even though the surface albedo varied over a range of 0.06 (for solar zenith angles varying between 42° and 76°), the data considered here show no correlation between the two quantities. This can be understood by the fact that *Henzing et al.* [2004] found their result for AOD = 0.25, which is at the high end of our range (cf. Figure 3; on average, our AOD is 30% lower). The effect of variable surface albedo on the diffuse irradiance is therefore likely to be less than the ±2 W/m$^2$ mentioned above.

[32] For an extensive sensitivity analysis, with focus on aerosol optical properties, the reader is referred to the work done by *Henzing et al.* [2004]. One should, however, bear in mind that these authors used MODTRAN for their simulations, which is a different model than the doubling adding model, DAK, used here.

## 5. Conclusion

[33] The study presented here shows that it is possible to obtain excellent closure for the direct, diffuse, and global irradiance using operational AERONET products and BSRN radiation measurements. The main model input consisted of the aerosol optical depth, single scattering albedo, asymmetry parameter, and water vapor column. Careful preparation of the model input and the use of the well-developed Doubling Adding KNMI (DAK) radiative transfer model led to average model–measurement differences of 2 W/m$^2$ (+0.2%) for the direct irradiance, 1 W/m$^2$ (+0.8%) for the diffuse irradiance, and 2 W/m$^2$ (+0.3%) for the global irradiance. Several sensitivity experiments, related to measurement uncertainties and model input assumptions, gave more insight in the required conditions for obtaining closure. High-quality measurements and accurate specification of the radiative transfer model are essential conditions for obtaining excellent closure. It is clear that uncertainties in the aerosol optical depth, single scattering albedo, and asymmetry parameter should be significantly less than 0.01, 0.1, and 0.1, respectively. The experiments based on using wavelength-independent values of the single scattering albedo and the asymmetry parameter showed that

spectral cancellation of errors in different parts of the solar spectrum may contribute to the good quality of broadband closure. As pointed out by *Michalsky et al.* [2006] a spectral evaluation of simulated irradiances, on the basis of well-calibrated spectrometer measurements, is needed to disclose spectral cancellation of errors.

[34] With the wealth of data obtained during the IMPACT campaign it will be possible to further examine in detail the assumptions that were made to run the DAK model. In particular, the model atmospheres could be further evaluated using ground-based and aircraft aerosol in situ measurements. The Raman lidar of RIVM provided vertical profiles of aerosol extinction that will be of great use.

[35] The strength of the method used here lies in its relative simplicity and the use of operational measurements. BSRN sites are located in different climatic zones and provide the high-quality radiation measurements needed to perform closure studies of the type presented here. About 15 BSRN sites have AERONET instruments, which will allow for similar studies under different climatic and aerosol conditions. Other networks, such as SKYNET, with its focus on eastern Asia, may also provide the data needed to extend the number of closure studies.

## References

Acarreta, J. R., J. F. De Haan, and P. Stammes (2004), Cloud pressure retrieval using the O$_2$-O$_2$ absorption band at 477 nm, *J. Geophys. Res.*, *109*, D05204, doi:10.1029/2003JD003915.

Anderson, G. P., et al. (1986), AFGL atmospheric constituent profiles, *Tech. Rep. AFGL-TR-86-0110*, Air Force Geophys. Lab., Hanscom AFB, Mass.

Barnard, J. C., and D. M. Powell (2002), A comparison between modeled and measured clear-sky radiative shortwave fluxes in Arctic environments, with special emphasis on diffuse radiation, *J. Geophys. Res.*, *107*(D19), 4383, doi:10.1029/2001JD001442.

Boersma, K. F., D. J. Jacob, H. J. Eskes, R. W. Pinder, J. Wang, and R. J. van der A (2008), Intercomparison of SCIAMACHY and OMI tropospheric NO$_2$ columns: Observing the diurnal evolution of chemistry and emissions from space, *J. Geophys. Res.*, *113*, D16S26, doi:10.1029/2007JD008816.

Bowker, D. E., R. E. Davis, D. L. Myrick, K. Stacy, and W. T. Jones (1985), Spectral reflectances of natural targets for use in remote sensing studies, *NASA Ref. Rep. 1139*, 184 pp., Greenbelt, Md.

Deepak, A., and H. E. Gerber (Eds.) (1983), World Climate Research report of the experts meeting on aerosols and their climatic effects, *WCP-55*, 107 pp., World Clim. Programme, Williamsburg, Va.

De Haan, J. F., P. B. Bosma, and J. W. Hovenier (1987), The adding method for multiple scattering computations of polarized light, *Astron. Astrophys.*, *183*, 371–391.

Dubovik, O., A. Smirnov, B. N. Holben, M. D. King, Y. J. Kaufman, T. F. Eck, and I. Slutsker (2000), Accuracy assessments of aerosol optical properties retrieved from Aerosol Robotic Network (AERONET) Sun and sky radiance measurements, *J. Geophys. Res.*, *105*, 9791–9806, doi:10.1029/2000JD900040.

Finsterle, W. (2006), WMO International Pyrheliometer Comparison IPC-X, 26 September–14 October 2005, Davos Switzerland, Final Report, *IOM Rep. 91., WMO/TD No. 1320*, 65 pp., World Meteorol. Org., Geneva.

Gueymard, C. A. (2001), Parameterized transmittance model for direct beam and circumsolar spectral irradiance, *Sol. Energy*, *71*, 325–346, doi:10.1016/S0038-092X(01)00054-8.

Gueymard, C. A. (2004), The sun's total and spectral irradiance for solar energy applications and solar radiation models, *Sol. Energy*, *76*, 423–453, doi:10.1016/j.solener.2003.08.039.

Halthore, R. N., and S. E. Schwartz (2000), Comparison of model estimated and measured diffuse downward irradiance at surface in cloud-free skies, *J. Geophys. Res.*, *105*, 20,165–20,177, doi:10.1029/2000JD900224.

Halthore, R. N., et al. (1997), Comparison of model estimated and measured direct-normal solar irradiance, *J. Geophys. Res.*, *102*, 29,991–30,002, doi:10.1029/97JD02628.

Henzing, J. S., W. H. Knap, P. Stammes, A. Apituley, J. B. Bergwerff, D. P. J. Swart, G. P. A. Kos, and H. M. ten Brink (2004), Effect of aerosols on the downward shortwave irradiances at the surface: Measurements versus calculations with MODTRAN4.1, *J. Geophys. Res.*, *109*, D14204, doi:10.1029/2003JD004142.

Kato, S., T. P. Ackerman, E. E. Clothiaux, J. H. Mather, G. G. Mace, M. L. Wesely, F. Murcray, and J. Michalsky (1997), Uncertainties in modeled and measured clear-sky surface shortwave irradiances, *J. Geophys. Res.*, *102*, 25,881–25,898, doi:10.1029/97JD01841.

Kato, S., T. P. Ackerman, J. H. Mather, and E. E. Clothiaux (1999), The k-distribution method and correlated-k approximation for a shortwave radiative transfer model, *J. Quant. Spectrosc. Radiat. Transfer*, *62*, 109–121, doi:10.1016/S0022-4073(98)00075-2.

Knap, W. H. (2008), Basic measurements of radiation at station Cabauw (2008-05), report, Koninklijk Nederlands Meteorol. Inst., De Bilt, Netherlands, doi:10.1594/PANGAEA.703322.

Knap, W. H, P. Stammes, and R. B. A. Koelemeijer (2002), Cloud thermodynamic phase determination from near-infrared spectra of reflected sunlight, *J. Atmos. Sci.*, *59*(1), 83–96, doi:10.1175/1520-0469(2002)059<0083:CTPDFN>2.0.CO;2.

Knap, W. H., L. C. Labonnote, G. Brogniez, and P. Stammes (2005), Modeling total and polarized reflectances of ice clouds: Evaluation by means of POLDER and ATSR-2 measurements, *Appl. Opt.*, *44*(19), 4060–4073, doi:10.1364/AO.44.004060.

Kuipers Munneke, P., C. H. Reijmer, M. R. van den Broeke, G. König-Langlo, P. Stammes, and W. H. Knap (2008), Analysis of clear-sky Antarctic snow albedo using observations and radiative transfer modeling, *J. Geophys. Res.*, *113*, D17118, doi:10.1029/2007JD009653.

McArthur, L. J. B. (2004), Baseline Surface Radiation Network (BSRN) operations manual–Version 2.1, *WMO/TD Rep.. 879*, World Clim. Res. Programme, World Meteorol. Org., Geneva.

Michalsky, J. J., G. P. Anderson, J. Barnard, J. Delamere, C. Gueymard, S. Kato, P. Kiedron, A. McComiskey, and P. Ricchiazzi (2006), Short-wave radiative closure studies for clear skies during the Atmospheric Radiation Measurement 2003 Aerosol Intensive Observation Period, *J. Geophys. Res.*, *111*, D14S90, doi:10.1029/2005JD006341.

Nowak, D., L. Vuilleumier, C. N. Long, and A. Ohmura (2008), Solar irradiance computations compared with observations at the Baseline Sur-face Radiation Network Payerne site, *J. Geophys. Res.*, *113*, D14206, doi:10.1029/2007JD009441.

Nyeki, S., C. Wehrli, and J. Gröbner (2009), Aerosol optical depth inter-comparison campaigns at European ''super-sites'' within the EU 6th Framework EUSAAR program, Annual Report 2008, Phys. Meteorol. Observ. Davos, Davos, Switzerland.

Ohmura, A., et al. (1998), Baseline Surface Radiation Network (BSRN/WCRP): New precision radiometry for climate research, *Bull. Am. Meteorol. Soc.*, *79*, 2115–2136, doi:10.1175/1520-0477(1998)079<2115:BSRNBW>2.0.CO;2.

Roebeling, R. A., H. M. Deneke, and A. J. Feijt (2008), Validation of cloud liquid water path retrievals from SEVIRI using one year of CloudNET observations, *J. Appl. Meteorol. Climatol.*, *47*, 206–222, doi:10.1175/2007JAMC1661.1.

Shi, Y., and C. N. Long (2002), Techniques and methods used to determine the best estimate of radiation fluxes at SGP central facility, in *Proceedings of the Twelfth ARM Science Team Meeting*, edited by D. Carrothers, U.S. Dep. of Energy, Richland, Wash.

Stammes, P. (2001), Spectral radiance modelling in the UV-visible range, in *IRS 2000: Current Problems in Atmospheric Radiation*, edited by W. L. Smith and Y. M. Timofeyev, pp. 385–388, A. Deepak, Hampton, Va.

Stammes, P., J. F. de Haan, and J. W. Hovenier (1989), The polarized internal radiation field of a planetary atmosphere, *Astron. Astrophys.*, *225*, 239–259.

Stoffel, T. (2005), Solar Infrared Radiation Station (SIRS) Handbook, *Tech. Rep., ARM TR-025*, 29 pp., Atmos. Radiat. Meas. Program, U.S. Dep. of Energy, Washington, D. C. (Available at http://www.arm.gov.)

Veefkind, J. P., J. F. de Haan, E. J. Brinksma, M. Kroon, and P. F. Levelt (2006), Total ozone from the Ozone Monitoring Instrument (OMI) using the DOAS technique, *IEEE Trans. Geosci. Remote Sens.*, *44*, 1239–1244, doi:10.1109/TGRS.2006.871204.

Veihelmann, B., P. F. Levelt, P. Stammes, and J. P. Veefkind (2007), Simulation study of the aerosol information content in OMI spectral reflectance measurements, *Atmos. Chem. Phys.*, *7*, 3115–3127.

Wang, P., W. H. Knap, P. Kuipers Munneke, and P. Stammes (2009), Clear-sky atmospheric radiative transfer: A model intercomparison for shortwave irradiances, in *Current Problems in Atmospheric Radiation (IRS 2008): Proceedings of the International Radiation Symposium (IRC/IAMAS)*, edited by T. Nakajima and M. A. Yamasoe, pp. 125–128, Springer, New York.

———————————

W. H. Knap, P. Stammes, and P. Wang, Royal Netherlands Meteorological Institute, P.O. Box 201, NL-3730 AE De Bilt, Netherlands. (knap@knmi.nl)

P. Kuipers Munneke, Institute for Marine and Atmospheric Research, Utrecht University, P.O. Box 8000, NL-3508 TA Utrecht, Netherlands.